ЖУРНАЛ СТРУКТУРНОЙ ХИМИИ

2016. Том 57, № 5 *Июнь – июль* *С. 916 – 922*

UDC 541.67:546.74

STRUCTURES AND MAGNETIC PROPERTIES OF Ni_n (n = 36—40) CLUSTERS FROM FIRST-PRINCIPLES CALCULATIONS

W. Song[1], B. Wang[1], K. Guo[3], W. Zhang[2]

[1]*Physics and Electronic Engineering Department, Xinxiang University, Xinxiang, P. R. China*
E-mail: chemsw@163.com
[2]*International Joint Research Laboratory of Nano-Micro Architecture Chemistry and Institute of Theoretical Chemistry, Jilin University, Changchun, Jilin, P. R. China*
E-mail: zhangw_bxx@jlu.edu.cn
[3]*The Shale Oil Plant Fushun Mining Group Co., Ltd, Fushun, P. R. China*

Received June, 15, 2015

A genetic algorithm (GA) coupled with a tight-binding (TB) interatomic potential is used to search for the low-energy structures of medium-sized Ni_n (n = 36—40) clusters. Structural candidates obtained from our GA search are further optimized with first-principles calculations. The medium-sized nickel clusters ranging from 36 to 40 atoms are found to favor the double-icosahedron-based structures with a Ni_7 core (a pentagonal bipyramidal structure) except Ni_{38} cluster. The lowest-energy structure of Ni_{38} can be considered to be a magic cluster, which is a typical face-centered cubic structure with large stability and magnetic moment.

DOI: 10.15372/JSC20160504

K e y w o r d s: nickel clusters, first-principle, magnetic properties.

INTRODUCTION

Atomic clusters are envisioned as playing a crucial role in a number of industrial applications such as catalysis, electronics, and optics [1—3]. The research field of clusters, particularly microclusters, has shown a rapid development in both experimental and theoretical investigations in the last decade. In particular, studies of transition metal clusters have attracted much interest. However, the properties of transition metal clusters are often different from those of the corresponding bulk materials, at least in the small size range they can show a strong dependence on the cluster size. Therefore in order to understand the physical and chemical properties such as catalysis, magnetic devices, and cluster assembled interfaces, it is undoubtedly important to obtain the geometrical structures of transition metal clusters [4—10]. Among 30 kinds of pure transition metal clusters, nickel clusters are the primary target of many research groups because of their extensive catalytic and important magnetic properties. However, the lowest-energy structure determination is usually a very difficult task even for clusters containing a few tens of atoms due to the rapidly increasing local minima as well as the number of structural parameters with increasing cluster size. Especially for transition metal clusters, this becomes even more complicated owing to the abundance of low-lying electron states and the delocalization of *d* electrons. Although there is a considerable improvement in the experimental techniques, the production and/or investigation of isolated microclusters of transition metal clusters is still difficult. Therefore, theoretical and computational predictions of cluster structures are important. Several studies focusing on the structures and properties of nickel clusters have been conducted. For example, the systematic study on the ground state electronic structure and magnetic properties of Ni_n (n = 2—39

and 55) clusters are performed using the density functional calculation with the local spin-density approximation [11]. The stable geometries and magnetic moments of Ni_n (n = 10—60) clusters were determined using the first principles method with ultrasoft pseudopotentials [12]. Within a rather general tight-binding framework, the magnetic properties of Ni_n clusters with (n = 9—60) have been studied [13]. Atomic clusters of 13, 55, and 147 Fe, Co, and Ni atoms with several values of the total magnetic moment were scanned, and the total energy minimum with respect to the total magnetic moment was searched using *ab initio* calculations based on spin-polarized density functional theory [14]. The geometries and magnetic moments of nickel clusters (Ni_n) as a function of the cluster size in the range 5—60 have been studied with a self-consistent tight-binding method considering 3*d*, 4*s*, and 4*p* valence electrons [15] and so on [16—20]. Although the previous studies revealed the structures and properties of nickel clusters, the most stable structures were not determined using the first-principles calculation, especially for more than 35 atoms.

In this paper we first apply a genetic algorithm with the tight-binding potential (GA/TB) method to search for low-lying structures. The candidate structures obtained from the GA/TB search were further refined by the DFT-PBE calculations. Apart from investigating some of the most stable structures, we also performed systematic calculations to provide a more comprehensive understanding of the growth pattern of stable structures and studied the binding energy and magnetic properties of nickel clusters in the range of 36—40 atoms.

COMPUTATIONAL METHODS

The GA method is based on the principles of natural evolution, which is an efficient computational tool for global geometry optimizations of clusters [21]. In this paper, we use a combination of the genetic algorithm (GA) with the tight-binding (TB) Ni potential and first-principles calculations for the global structural search for Ni clusters with 36—40 atoms. First, an unbiased search for the low-lying structures of Ni_n (n = 36—40) clusters was performed using the GA/TB method. The method is widely used in the calculations of materials and clusters [22]. The TB Ni potential including *d* orbitals, which was used in this work, was developed similar to the environment-dependent TB potential with *s* and *p* orbitals, which was proposed by Wang et al. [23—24], and the parameters in the TB potential have been kept updating on-the-fly along with the GA/TB search to match the DFT-PBE energy orders of different isomers of the Ni_n clusters with different sizes. At first, a pool of p = 20 structures for a given cluster size n is generated; then in each subsequent generation, mating operations cutting *A* and *B* into two halves and permuting their lower halves are used to generate offspring structures. We also input some hand-made structures into the GA search in order to enrich the types of low-energy structures. At the end of the global structural search, 20 low-lying structures remained as potential candidates, which were further optimized using the DFT method implemented in the VASP code [25] with the spin polarized PBE (Perdew, Burke, and Ernzerhof) gradient-corrected exchange-correlation functional method. The cutoff energy of plane waves (PW) in the calculations was taken to be 269.5 eV. A simple cubic supercell with a size of 20 Å was used. The geometry optimization of each isomer was carried out until the energy was converged to an accuracy of 10^{-4} eV.

RESULTS AND DISCUSSION

Structures of Ni_n (n = 36—40) clusters. The low-energy structures of Ni_n (n = 36—40) clusters are shown in Fig. 1, in which the growth motif for Ni_n (n = 36—40) has been revealed. All the geometries and relative energies presented in this work resulted from the DFT-PBE calculations. As one can see, the lowest-energy structures of the Ni_n clusters (n = 36—40) exhibit the double-icosahedron-based geometries except the Ni_{38} cluster. The lowest-energy structure of Ni_{38} is a typical face-centered cubic (fcc) structure. From our previous research [19], the number of central atoms of the lowest-energy isomers tends to increase as a function of the cluster size. The number of central atoms is two endohedral atoms for Ni_{20}—Ni_{22}, three endohedral atoms for Ni_{23}—Ni_{25}, four endohedral atoms (Ni_4 with a tetrahedral structure, Fig. 2, *a*) for Ni_{26}—Ni_{31}, five endohedral atoms (Ni_5 with a trigonal bipyramidal structure, Fig. 2, *b*) for Ni_{32}—Ni_{33}, and six endohedral atoms (Ni_6 with a square bipyramidal structure,

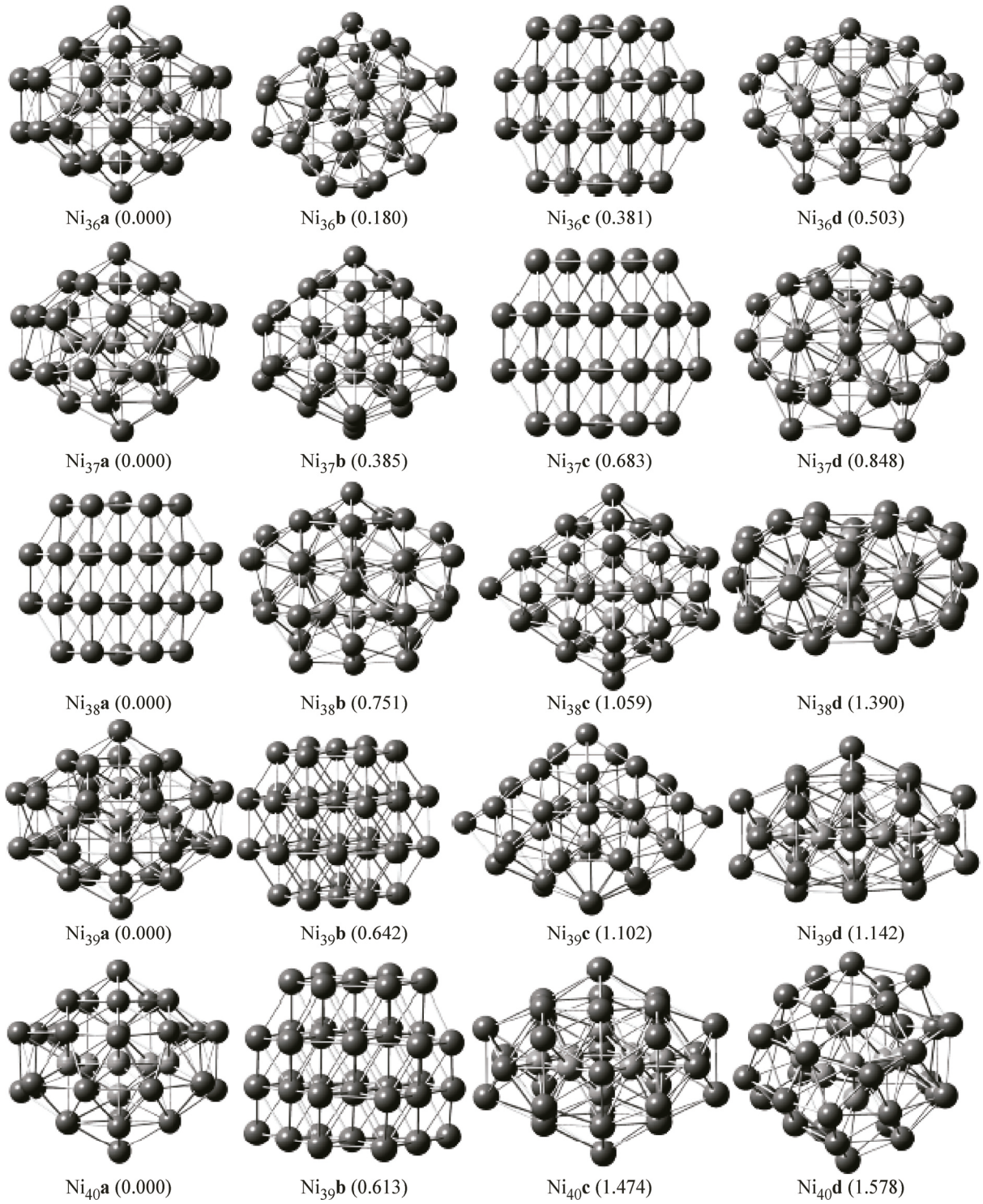

Fig. 1. Low-energy isomers of Ni_n (n = 36—40) clusters and relative energies (in eV) calculated at the DFT-PBE level

Fig. 2, *c*) for Ni_{34}—Ni_{35}, respectively. In this work we can observe that the lowest-energy structures of $Ni_{36—40}$ clusters possess a Ni_7 core with a pentagonal bipyramidal structure (Fig. 2, *d*), except the Ni_{38} cluster. The distance between the two vertices of the pentagonal bipyramidal structure is 2.39, 2.41, 2.48, and 2.49 Å for the Ni_{36}, Ni_{37}, Ni_{39}, and Ni_{40} cores respectively. The distances increase monotonically as a function of the cluster size.

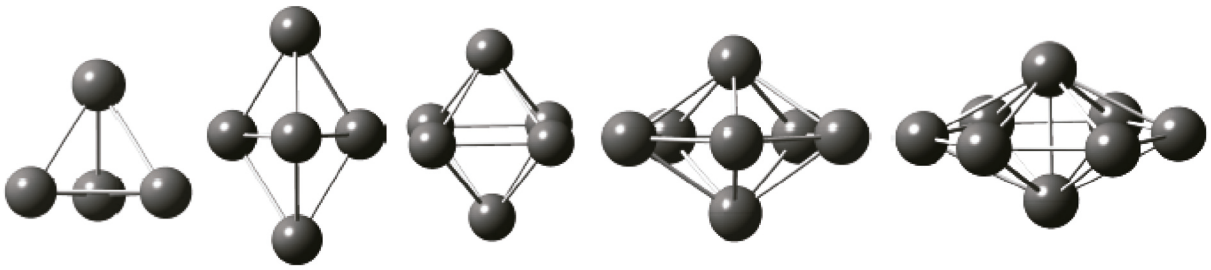

Fig. 2. Small stable nickel cluster structures acting as large cluster cores

A detailed comparison of the low-energy isomers is discussed as follows. The Ni_{36}**a** structure is viewed as adding atoms to the waist of the double-icosahedron structure with C_s symmetry. Ni_{36}**b** is a small distorted double-icosahedron-like structure with a Ni_5 core and the relative energy is 0.180 eV higher than that of Ni_{36}**a**. The third isomer Ni_{36}**c** is formed by removing two atoms from the fcc structure of Ni_{38}**a**. The Ni_{36}**d** structure is very interesting and looks like a loom. Ni_{37}**a** is obtained by adding one atom to Ni_{36}**a** to fill the vacancy for the back of Ni_{36}**a** showing the C_2 symmetry. As can be seen from the Fig. 1, the Ni_{37}**b**, Ni_{37}**c**, and Ni_{37}**d** isomers are formed by adding one atom to Ni_{36}**b**, Ni_{36}**c**, and Ni_{36}**d**, respectively. From our discussion it can be seen that the lowest-energy structures of $Ni_{36—37}$ clusters exhibit the double-icosahedron-based geometries. However, the most stable structural motif of Ni_{38} is different from the double-icosahedron-based structure, which is found to be a typical fcc fragment and composed of four parallel arranged pieces of fcc (111) faces, in agreement with the experiment of Riley and co-workers [26] and the theoretical calculation [15, 27]. The double-icosahedron-based Ni_{38}**b** and Ni_{38}**c** isomers are viewed as adding one atom to Ni_{37}**d** and Ni_{37}**a**, but the relative energies are 0.751 and 1.059 eV higher than that of Ni_{38}**a**, respectively. And Ni_{38}**d** is found to be a new structure which looks like two rotating tires. Then, by attaching one atom at the side face in the waist of Ni_{38}**c**, Ni_{39}**a** is form with the C_5 symmetry. Ni_{40}**a** with the C_s symmetry is obtained by attaching one more atom to the pentagonal ring in the top of the double-interpenetrating icosahedron of Ni_{39}**a**, so that the pentagonal ring is replaced by the hexagonal ring. Ni_{39}**d** and Ni_{40}**c** are very similar with the addition of one and two atoms to the top and bottom surfaces of the Ni_{38}**d** cluster respectively. The structure of Ni_{40}**c** can also be viewed from another angle as shown in Fig. 3, showing that Ni_{40}**c** can be considered to be composed of two interpenetrating 22-atom double-icositetrahedra (with three parallel hexagonal rings) with the core fragment growing from Ni_7 to Ni_8 (Fig. 2, *e*), which looks like a rotating Ferris wheel. Unlike Ni_n (n = 31—35) clusters [19] which favor double-icosahedron-like structures with a severe deformation, the increased $Ni_{36—40}$ clusters prefer compact near-spherical structures with a better symmetry. Ni_{38} has a tendency to grow in bulk-like stacking as a magic number cluster; the lowest-energy structure of Ni_{38} is a typical fcc structure.

Relative stabilities. In order to understand the relative stabilities of Ni_n (n = 31—35) clusters, we have analyzed the binding energies per atom (E_b) and second energy differences ($\Delta_2 E$). The calculated

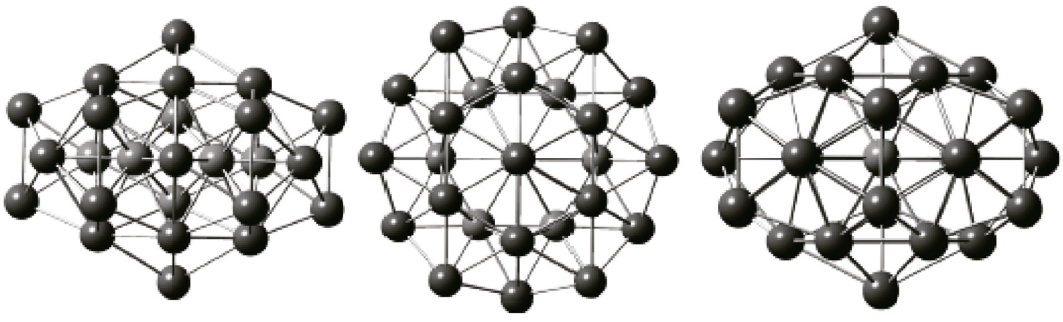

Fig. 3. Low-energy isomer of the Ni_{40}**c** cluster from different visual angles

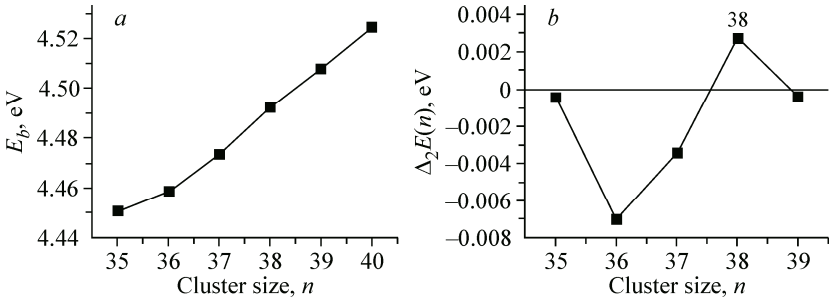

Fig. 4. Binding energy per atom, defined by $E_b = [E_{total}(Ni_n) - nE(Ni)]/n$ of Ni_n**a** ($n = 35$—40) (*a*). Second energy difference defined by $\Delta_2E(n) = E(n + 1) + E(n - 1) - 2E(n)$ of Ni_n**a** ($n = 35$—39) (*b*)

results are shown in Fig. 4, *a* and *b*. E_b of Ni_n is calculated according to the following definition:

$$E_b = [E_{total}(Ni_n) - nE(Ni)]/n,$$

where $E_{total}(Ni_n)$ is the total energy of Ni_n and $E(Ni)$ is the energy of a free Ni atom. From Fig. 4, *a* it can be seen that the binding energy per atom of nickel clusters increases monotonically as a function of the cluster size. To clarify the relative stabilities of the clusters, we also calculated the second difference of the cluster, which is defined by

$$\Delta_2E(n) = E(n + 1) + E(n - 1) - 2E(n).$$

According to this definition, the clusters with positive Δ_2E are more stable than those with negative Δ_2E. Calculated Δ_2E for the Ni_n clusters are plotted in Fig. 4, *b*. We can see that the curve exhibits an oscillating behavior, and Ni_{38} corresponds to the local maxima on the Δ_2E curve, showing that Ni_{38} is a relatively more stable cluster. It is further explained that the stability of the fcc structure for the Ni_{38} cluster is greater than that of the double-icosahedron-based structure.

Magnetic properties. In principle, both spin and orbital magnetic moment make a contribution to the total magnetic moment in any system. The spin magnetic moment arises from the alignment of electron spins and the orbit magnetic moment is induced by the electron motion in a circular orbit around a nucleus. Nickel clusters are typically ferromagnetic 3*d* group transition metal clusters. The configuration of the Ni atom is $3d^84s^2$. According to the Pauli exclusion principle and the Hund rule, two unpaired 3*d* electrons of the Ni atom contribute to its magnetic property. Recent experiments have found that the orbital moments can be as large as 10 to 30 % of the spin moment [28]. Therefore for 3*d* group transition metals, the magnetic moment caused by the unpaired electron orbital motion is relatively small. The atomic total magnetic moment depends mainly on the electronic spin magnetic moment. As shown in Fig. 5, the trend of the magnetic moment obtained from our calculation is in good agreement with the experimental results [29], except the Ni_{38} cluster. Fig. 5 also shows that the magnetic moments are smaller than the experiment data. The reason is that we did not include the effect of orbital moments in the calculation. However, the magnetic moment of the Ni_{38}**a** cluster is maximum, which is inconsistent with the previous experimental results [29] due to the special fcc structure of the Ni_{38} cluster. Thus, it can be seen that the magnetic moment is affected by cluster structures. To further understand the impact of the structure on the magnetic moment, we can compare the total magnetic moment of Ni_n ($n = 36$—40) clusters with double-icosahedron-based and fcc structures in Table 1. Firstly, we can observe that the magnetic moments are highest for the most stable structures in all the clusters, which provides a theoretical basis for the choice of the magnetic material. Secondly, it can be seen that the icosahedral clusters typically exhibit higher magnetic moments

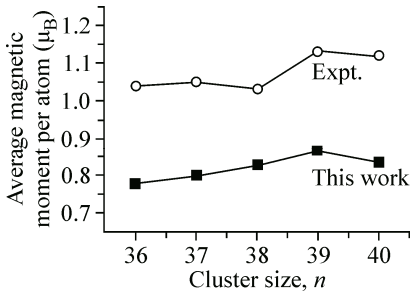

Fig. 5. Comparison between the calculated average magnetic moment per atom of Ni_n ($n = 36$—40) clusters and the experimental results of [29]

than the fcc clusters of the same size, except the Ni_{38} cluster. Finally, the average magnetic moment of Ni_{38}**c** (double-icosahedron-based structure) is $0.742\mu_B$, which is lowest in Ni_n (n = 36—40) clusters, it being in agreement with the previous study [29]. Therefore, we can consider that the magnetic moment is highest and lowest for the fcc structure and the double-icosahedron-based structure of the Ni_{38} cluster, respectively.

Table 1

Comparison of the total magnetic moment of Ni_n (n = 36—40) *clusters with double-icosahedron-based and* fcc *structures*

Magnetic moment (μ_B)	Double-icosahedron-based structure	Face-centered cubic structure
Ni_{36}	27.992	26.200
Ni_{37}	29.587	27.956
Ni_{38}	28.202	32.891
Ni_{39}	33.132	33.021
Ni_{40}	33.409	33.219

CONCLUSIONS

The lowest-energy structures of the Ni_n (n = = 36—40) clusters were located by a combination method of the GA/TB search and first-principles calculations at the DFT-PBE level. The growth pattern of Ni clusters in the size range from 36 to 40 atoms favors the double-icosahedron-based structures with a Ni_7 core (a pentagonal bipyramidal structure), except the Ni_{38} cluster. They can be formed by adding atoms to the waist of the double-icosahedron structure. The lowest-energy structure of Ni_{38} is a typical fcc structure. We also discussed the properties of these nickel clusters, including the binding energies per atom, second energy differences, and magnetic moments. The binding energy per atom of nickel clusters increases monotonically as a function of the cluster size. It can be found that the thermodynamic stability of the Ni_n clusters have an oscillation character, where Ni_{38} exhibits a higher stability than its neighbors. The trend of the magnetic moment obtained from our calculation is in good agreement with the experimental results, except the Ni_{38} cluster.

This work is supported by the National Natural Science Foundation of China for financial support (Grant Nos.: 20921002, 21273219, 21203174) and Jilin Province (20130522141JH). The computational resource is partly supported by the Performance Computing Center of Jilin University, China. Ames Laboratory is operated for the U.S. Department of Energy by Iowa State University under Contract No. DE-AC02-07CH11358. This work was also supported by the Director for Energy Research, Office of Basic Energy Sciences including a grant of computer time at the National Energy Research Supercomputing Center (NERSC) in Berkeley.

REFERENCES

1. *Schmid G., Bäumle M., Geerkens M., Heim I., Osemann C., Sawitowski T.* // Chem. Soc. Rev. – 1999. – **28**. – P. 179 – 185.
2. *Aiken J.D., Finke R.G.* // J. Mol. Catal. A: Chem. – 1999. – **145**. – P. 1 – 44.
3. *Migowski P., Dupont J.* // Chem. Eur. J. – 2007. – **13**. – P. 32 – 39.
4. *Lecoultre S., Rydlo A., Buttet J., Felix C., Gilb S., Harbich W.* // J. Chem. Phys. – 2011. – **134**. – 184504(1) – (6).
5. *Itoh M., Kumar V., Adschiri T., Kawazoe Y.* // J. Chem. Phys. – 2009. – **131**. – 174510(1) – (19).
6. *Xu X.S., Yin S.Y., Moro R., de Heer W.A.* // Phys. Rev. Lett. – 2005. – **95**. – 237209(1) – (4).
7. *Gruene P., Rayner D.M., Redlich B., van der Meer A.F.G., Lyon J.T., Meijer G., Fielicke A.* // Science. – 2008. – **321**. – P. 674 – 676.
8. *Li J., Li X., Zhai H.J., Wang L.S.* // Science. – 2003. – **299**. – P. 864 – 867.
9. *Ma Q.M., Xie Z., Wang B.R., Liu Y., Li Y.C.* // Solid State Commun. – 2011. – **151**. – P. 806 – 810.
10. *Datta S., Kabir M., Dasgupta1 T.S.* // Phys. Rev. B. – 2011. – **84**. – 075429(1) – (8).
11. *Duan H.M., Gong X.G., Zheng Q.Q.* // J. Appl. Phys. – 2001. – **89**. – P. 7308 – 7310.
12. *Yao Y.H., Gu X., Ji M., Gong X.G., Wang D.S.* // Phys. Lett. A. – 2007. – **360**. – P. 629 – 631.
13. *Wan X.G., Zhou L., Dong J.M., Lee T.K., Wang D.S.* // Phys. Rev. B. – 2004. – **69**. – 174414(1) – (14).
14. *Singh R., Kroll P.* // Phys. Rev. B. – 2008. – **78**. – 245404(1) – (9).
15. *Aguilera-Granja F., Bouarab S., López M.J., Vega A., Montejano-Carrizales J.M., Iñiguez M.P., Alonso J.A.* // Phys. Rev. B. – 1998. – **57**. – P. 12469 – 12475.
16. *Grigoryan V.G., Springborg M.* // Phys. Chem. Chem. Phys. – 2001. – **3**. – P. 5135 – 5139.

17. *El-Bayyari Z.* // J. Mol. Struct.: THEOCHEM. – 2005. – **716**. – P. 165 – 174.
18. *Song W., Lu W.C., Zang Q.J., Wang C.Z., Ho K.M.* // Int. J. Quantum Chem. – 2012. – **112**. – P. 1717 – 1724.
19. *Song W., Lu W.C., Zang Q.J., Li Q.X.* // Chem. Res. Chin. Univ. – 2012. – **28**, N 2. – P. 291 – 294.
20. *Song W., Lu W.C., Wang C.Z., Ho K.M.* // Comput. Theor. Chem. – 2011. – **978**. – P. 41 – 46.
21. *Peterson M.R., Doom T.E., Raymer M.L.* // Lect. Notes Comput. Sci. Eng. – 2004. – **3102**. – P. 426 – 437.
22. *Wang C.Z., Ho K.M.* // Handb. Mater. Model. – 2005. – **1**. – P. 307.
23. *Wang C.Z., Pan B.C., Ho K.M.* // J. Phys.: Condens. Matter. – 1999. – **11**. – P. 2043 – 2048.
24. *Tang M.S., Wang C.Z., Chan C.T. et al.* // Phys. Rev. B. – 1996. – **53**. – P. 979.
25. (a) *Kresse G., Hafner J.* // Phys. Rev. B. – 1993. – **47**. – P. 558 – 561. (b) *Kresse G., Furthmuller J.* // Phys. Rev. B. – 1996. – **54**. – P. 11169.
26. *Parks E.K., Niemann G.C., Kerns K.P., Riley S.J.* // J. Chem. Phys. – 1997. – **107**. – P. 1861 – 1865.
27. *Xiang Y., Sun D.Y., Gong X.G.* // J. Phys. Chem. A. – 2000. – **104**. – P. 2746 – 2751.
28. *Lau J.T., Föhlisch A., Martins M., Nietubyc R., Reif M., Wurth W.* // New J. Phys. – 2002. – **4**. – 98(1) – (4).
29. *Apsel S.E., Emmert J.W., Deng J., Bloomfield L.A.* // Phys. Rev. Lett. – 1996. – **76**. – P. 1441 – 1444.